Cerebellar output controls the occurrence of generalized spike-and-wave discharges in epileptic cerebral cortex

Lieke Kros[a], Oscar H.J. Eelkman Rooda[a], Jochen K. Spanke, Parimala Alva, Marijn N. van Dongen, Athanasios Karapatis, Else A. Tolner[4], Christos Strydis, Neil Davey, Beerend H.J. Winkelman, Mario Negrello, Wouter A. Serdijn, Volker Steuber, Arn M.J.M. van den Maagdenberg, Chris I. De Zeeuw and Freek E. Hoebeek

[a]*These authors contributed equally.*

Annals of Neurology, 77(6), 1027-1049. DOI 10.1002/ana.24399

ABSTRACT

Objective: Disrupting thalamocortical activity patterns has proven to be a promising approach to stop generalized spike-and-wave discharges (GSWDs) characteristic of absence seizures. Here, we investigated to what extent modulation of neuronal firing in cerebellar nuclei (CN), which are anatomically in an advantageous position to disrupt cortical oscillations through their innervation of a wide variety of thalamic nuclei, is effective in controlling absence seizures.

Methods: Two unrelated mouse models of generalized absence seizures were used; the natural mutant *tottering*, which is characterized by a missense mutation in *Cacnala*, and inbred *C3H/HeOuJ*. While simultaneously recording single CN neuron activity and electrocorticogram (ECoG) in awake animals, we investigated to what extent pharmacologically increased or decreased CN neuron activity could modulate GSWD occurrence and short-lasting on-demand CN stimulation could disrupt epileptic seizures.

Results: We found that a subset of CN neurons shows phase-locked oscillatory firing during GSWDs and that manipulating this activity modulates GSWD occurrence. Inhibiting CN neuron action potential firing by local application of the GABAA-agonist muscimol increased GSWD occurrence up to 37-fold, whereas increasing the frequency and regularity of CN neuron firing with the use of gabazine decimated its occurrence. A single short-lasting (30–300 ms) optogenetic stimulation of CN neuron activity abruptly stopped GSWDs, even when applied unilaterally. Using a closed-loop system GSWDs were detected and stopped within 500 ms.

***Interpretation*:** CN neurons are potent modulators of pathological oscillations in thalamocortical network activity during absence seizures and their potential therapeutic benefit for controlling other types of generalized epilepsies should be evaluated.

3.1. INTRODUCTION

Absence epilepsy is one of the most prevalent forms of generalized epilepsy among children and is characterized by sudden periods of impaired consciousness and behavioral arrest[1,2]. Like other types of generalized epilepsies, absence seizures are electrophysiologically defined by oscillatory activity in cerebral cortex and the thalamic complex[3]. Thalamocortical oscillations are primarily caused by excessive cortical activity and can be identified in the electrocorticogram (ECoG) as generalized spike-and-wave discharges (GSWDs)[3,4]. The underlying excessive cortical activity not only excites thalamic neurons, but also provides potent bisynaptic inhibition by means of cortical axonal collaterals to the inhibitory reticular thalamic nucleus[3,5–7]. Excess tonic GABA-mediated inhibition in thalamus may also contribute to absence seizures[3,7,8]. Oscillatory cortical activity thereby poses a dual excitation-inhibition effect on thalamic neurons, which drives thalamocortical network oscillations[5,7–9].

Recent studies in several rodent models indicate that direct stimulation of thalamic nuclei[10] or cerebral cortex[11] can be effective in disrupting thalamocortical oscillations and thereby stopping generalized oscillations in thalamocortical networks, such as GSWDs. Apart from direct interventions in thalamus and cortex, synaptic thalamic afferents can affect the balance in excitation and inhibition and thereby potentially mediate thalamocortical oscillations. One of the initial stimulation sites to prevent seizures in epileptic patients was the cerebellar cortex[12–18]. Yet, as shown in three controlled, blind studies[19–21], the impact of these cerebellar surface stimulations was highly variable and probably reflects irregularities in the converging inputs from superficial and deeper parts of the cerebellar cortex neurons in the cerebellar nuclei (CN)[22].

Given the considerable divergence of excitatory axonal projections from the cerebellar nuclei (CN) to a wide range of motor, associative and intralaminar thalamic nuclei[4,6,23–29], we considered this region an ideal candidate to effectively modulate thalamocortical oscillations. We hypothesized that altering the firing patterns of CN neurons should affect GSWD occurrence. To test this hypothesis we utilized homozygous *tottering* (*tg*) mice that frequently show absence seizures and harbor a P601L missense mutation in the *Cacna1a* gene that encodes the pore-forming α_{1A}-subunit of voltage-gated $Ca_V2.1$ Ca^{2+} channels[30,31]. Once we established that *tg* CN neurons showed oscillatory action potential firing patterns comparable to that found in rat models for absence epilepsy[32], we assessed the effect of increasing or decreasing CN neuronal firing on GSWD occurrence by local pharmacological interventions using modulators of GABAA-mediated neurotransmission. In addition, we generated a closed-loop detection system for on-demand optogenetic stimulation to stimulate CN neurons with millisecond precision. Finally, to exclude the

possibility that our design of intervention is tailored to the specific pathophysiology of *tg* mice we extended our key experiments to an unrelated mouse model for absence epilepsy; the *C3H/HeOuJ* inbred mouse line[33].

3.2. MATERIALS AND METHODS

All experiments were performed in accordance with the European Communities Council Directive. Protocols were reviewed and approved by local Dutch experimental animal committees (DEC).

3.2.1. Animals

Data were collected from 4-to 30-week-old homozygous and wild-type littermates of the natural mutant *tottering* (mouse symbol *tg*) mice and 8-to 10-week-old inbred *C3H/HeOuJ* mice. Male and female *tg* and wild-type littermates were bred using heterozygous parents. The colony, which was originally obtained from Jackson laboratory (Bar Harbor, ME, USA), was maintained in C57BL/6NHsd purchased from Harlan laboratories (Horst, Netherlands). Conformation of the presence of the *tg* mutation in the *Cacna1a* gene was obtained by PCR using 5′-TTCTGGGTACCAGATACAGG-3′ (forward) and 5′-AAGTGTCGAAGTTGGTGCGC-3′ (reverse) primers (Eurogentech, Seraing, Belgium) and subsequent digestion using restriction enzyme *NsbI* at the age of P9 – P12. Male inbred *C3H/HeOuJ* mice were purchased from Charles River Laboratories (Wilmington, MA, USA).

3.2.2. Experimental procedures

Surgery

Mice were anesthetized with isoflurane (4% in 0.5 L/min O2 for induction and 1.5% in 0.5 L/min O2 for maintenance). The skull was exposed, cleaned and treated with OptiBond All-In-One (Kerr Corporation; Orange, CA, USA) to ensure adhesion of a light-curing hybrid composite (Charisma; Heraeus Kulzer, Hanau, Germany) to the skull to form a pedestal. Subsequently, five 200-µm teflon-coated silver ball tip electrodes (Advent research materials, Eynsham, Oxford, UK) or five 1-mm stainless steel screws were subdurally implanted for cortical recordings by ECoG. Four of the electrodes were bilaterally positioned above the primary motor cortex (+1 mm AP; ± 1 mm ML relative to bregma) and primary sensory cortex (–1 mm AP; ± 3.5 mm ML). A fifth electrode was placed in the rostral portion of the interparietal bone to serve as reference (–1 mm AP relative to lambda). The electrodes and their connectors were fixed to the skull and embedded in a pedestal composed of the hybrid composite or dental acrylic (Simplex Rapid; Associated Dental Products, Kemdent works, Purton, Wiltshire, UK). To enable optogenetic control of neuronal

activity in CN, a subset of *tg* and *C3H/HeOuJ* mice received two small (~0.5 mm in diameter) craniotomies in the interparietal bone (-2 mm AP relative to lambda; ± 1.5–2 mm ML) to initially accommodate the injection pipette and later the optical fibers. CN were stereotactically injected bilaterally with 100–120 nL of the AAV2-hSyn-ChR2(H134R)-EYFP vector (kindly provided by Prof. K. Deisseroth (Stanford University) through the UNC vector core) at a rate of ~20 nL/min 3–6 weeks prior to recordings. To allow electrophysiological recordings from CN neurons, all mice received bilateral craniotomies (~2 mm diameter) in the occipital bone without disrupting the dura mater. Finally, a dental acrylic recording chamber (Simplex rapid) was constructed. The exposed tissue was covered with tetracycline-containing ointment (Terracortril; Pfizer, New York, NY, USA) and the recording chamber was sealed with bone wax (Ethicon, Somerville, NJ, USA). After surgery, the mice recovered for at least 5 days (or 3 weeks in case of virally-injected mice) in their home cage and were allowed two ~3-hr sessions on consecutive days during which the mice were left undisturbed to accommodate to the setup.

Electrophysiological recordings

During the accommodation session the animals' motor behavior was visually inspected for behavioral correlates of the oscillatory cortical activity during episodes of generalized spike-and-wave-discharges (GSWDs). No consistent patterns of movement were identified during such epileptic activity, as described before in *tg* and other rodent models of absence epilepsy[30,32,34] Recordings were performed in awake, head-fixed animals, lasted no longer than 4 consecutive hours and were performed during various times of day. No consistent pattern was identified in ECoG frequency spectra with respect to the day-night cycle[35]. While being head-restrained, mice were able to move all limbs freely. Body temperature was supported using a homeothermic pad (FHC, Bowdoin, ME, USA). For extracellular single unit recordings, custom-made, borosilicate glass capillaries (OD 1.5 mm, ID 0.86 mm; resistance 8–12 MΩ; taper length~8 mm; tip diameter ~1 µm) (Harvard Apparatus, Holliston, MA, USA) filled with 2 M NaCl were positioned stereotactically using an electronic pipette holder (SM7; Luigs & Neumann, Ratingen, Germany). CN were localized by stereotactic location as well as the characteristic sound and density of neuronal activity[36]. To record from medial CN (MCN), electrodes were advanced through vermal lobules 6–7 with 0° jaw angle relative to the inter-aural axis to a depth of 1.6–2.4 mm. To record from interposed nuclei (IN), electrodes were advanced through the paravermal or hemispheric part of lobules 6–7 using a yaw angle of ~10° relative to the inter-aural axis to a depth of 1.8–2.7 mm. To record from lateral CN (LCN), electrodes were advanced through the paravermal or hemispheric part of lobules 6–7 using a yaw angle of ~25° relative to the inter-aural axis to a depth of 2.7–4 mm. A subset of electrophysiological recording sites was

identifiable following Evans blue injections (see below) and confirmed the accuracy of our localization technique. ECoGs were filtered online using a 1–100 Hz band pass filter and a 50 Hz notch filter. Single-unit extracellular recordings and ECoGs were simultaneously sampled at 20 kHz (Digidata 1322A, Molecular Devices LLC., Axon Instruments, Sunnyvale, CA, USA), amplified, and stored for off-line analysis (CyberAmp & Multiclamp 700A, Molecular Devices LLC.).

Pharmacological modulation of CN neuronal action potential firing

In order to bilaterally target the CN for pharmacological intervention, their location was first determined as described above, after which we recorded one hour of 'baseline' ECoG. Next, a borosilicate glass capillary (Harvard Apparatus; tip diameter of ~5 μn) filled with either one of the following mixtures replaced the recording pipette to allow high spatial accuracy of the injection: to decrease CN neuronal action potential firing, we applied 0.5% muscimol ($GABA_A$-agonist; Tocris) dissolved in 1 M NaCl (Sigma-Aldrich); to increase CN neuronal action potential firing, we applied 100 μM gabazine ($GABA_A$-antagonist; Tocris) dissolved in 1 M NaCl; or 1 M NaCl for sham injections. The solution was bilaterally administered to CN by pressure injections of ~150 nL at a rate of ~50 nL/min following which one hour of post-injection ECoG was recorded. As an additional control, similarly-sized injections of saline with either gabazine or muscimol were administered to lobule 6 and 7 and Crus I and Crus II of the cerebellar cortex. The drugs were injected superficially (0.7–1 mm from the surface) to avoid spread to the CN. The locations of the injections were identified with the use of electrophysiological recordings and stereotactic coordinates and most (19 out of 26) CN injections were histologically confirmed using the fluorescence of Evans blue (1% in 1M saline; Fig. 3.S1)[37]. To verify the effects of muscimol, gabazine, and vehicle, we recorded extracellular activity in the injected area during 20–50 min after the injections. Immediately after acquiring the post-injection ECoG an overdose of sodium-pentobarbital (0.15 mL *i.p.*) was administered allowing transcardial perfusion (0.9% NaCl followed by 4% paraformaldehyde in 0.1 M phosphate buffer (PB); pH=7.4) to preserve the tissue for histological verification of the injections.

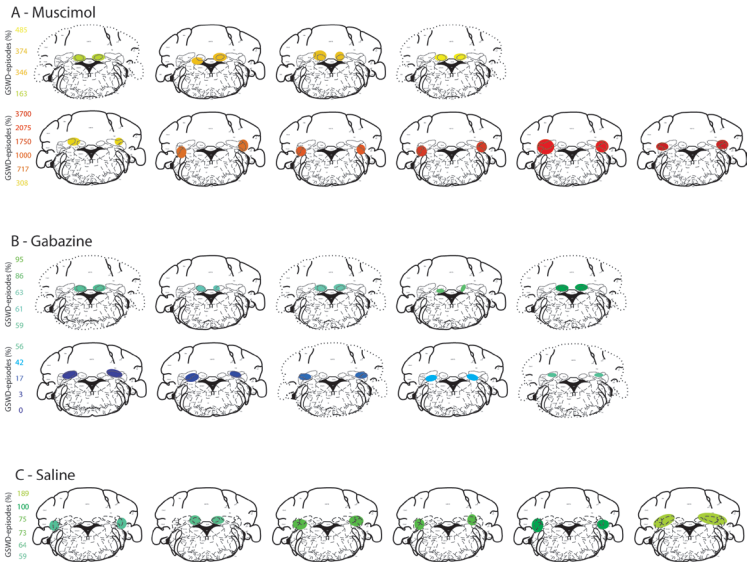

Fig. S1 *Schematic representation of the location of CN injections.*

*The location of injections of muscimol (**A**), gabazine (**B**) and saline (**C**) in the CN as verified by stereotactic coordinates and electrophysiological measurements (dashed cerebellar outlines) or by coordinates, activity and immunohistochemical (Evans blue) verification (solid cerebellar outlines). Note the consistent differences in the effects on GSWD-occurrence (color-coded; blue indicates decreased and red indicates increased GSWD-occurrence) between injections located in the MCN, IN and LCN.*

Optogenetic stimulation of CN neurons

Optic fibres (200 µm inner diameter; 0.39 NA) were placed ~200 µm from the injection site and connected to 470-nm or 590-nm LEDs, or ~200 µm above the brain, *i.e.*, 'wrong location'. Light intensity at the tip of the implantable fibre was 550±50 µW/mm^2 (measured after each experiment). Activation of LEDs by a single 30 – 300 ms pulse was triggered manually ('open-loop') or by a closed-loop detection system (as described below). In each mouse, 4 stimulation protocols were used: 1) bilateral stimulation (470 nm) 2) unilateral stimulation (470 nm); 3) bilateral stimulation (590 nm); and 4) bilateral stimulation (470 nm) with optical fibres outside of the CN (to exclude potential effects of visual input on the GSWD occurrence – see refs[30,32]). All hardware used for optogenetic stimulation was purchased from ThorLabs (Newton, NJ, USA). After the last experimental session, animals were sedated and perfused (as described above) to preserve tissue for histological verification of ChR2 expression.

Immunofluorescence
After perfusion, the cerebellum was removed and post-fixed in 4% paraformaldehyde in 0.1 M PB for 1.5 hr, placed in 10% sucrose in 0.1 M PB at 4°C overnight, and subsequently embedded in gelatine in 30% sucrose (in 0.1 M PB). Embedded brains were post-fixed for 2.5–3 hr in 30% sucrose and 10% formaldehyde (in MilliQ) and placed overnight in 30% sucrose (in 0.1 M PB) at 4°C. Forty-µm thick transversal slices were serially collected for immunofluorescent DAPI staining. Fluorescent images taken at 555 nm (Evans blue), 405 nm (DAPI) and 488–527 nm (GFP/YFP range) were utilized to confirm correct localization of the injections.

3.2.3. Data analyses

Offline GSWD detection
In order to accurately determine start and end of absence GSWDs and the locations of ECoG 'spikes' (negative ECoG peaks during episodes of GSWDs), a custom-written GSWD detection algorithm (LabVIEW, National Instruments, Austin, TX, USA) was used. In short, we detected those time points in the ECoG for which the first derivative of the filtered ECoG traces (3rd order Butterworth 1 Hz high-pass) changed polarity. The amplitude differences between each point and both its neighbors were summed in order to detect fast, continuous amplitude changes and potential GSWDs with a manually set amplitude threshold. Series of GSWDs were marked when: 1) five threshold-exceeding points appeared within 1 s; and 2) each of the intervals between the points was <300 ms. Furthermore, we separated GSWDs by applying the following four rules: 1) a point is the first spike of a GSWD-episode if there are no other spikes in the previous 300 ms; 2) a point is the last spike of a GSWD-episode if there are no other spikes in the next 350 ms; 3) the inter-GSWD-episode interval is ≥ 1s; and 4) the minimal GSWD duration is 1s.

GSWD definition
An ictal period is defined to start at the first ECoG spike of a GSWD and end at the last ECoG spike. Unless stated otherwise SWDs that lasted >1 s and appeared in both M1 and S1 were considered GSWD. An interictal period is defined as the time in between GSWDs starting 2s after one GSWD and ending 2s before the next GSWD.

Detection of action potentials in extracellular recordings
Extracellular recordings were included if activity was well-isolated and held stable for >100 s. Action potential detection in extracellular traces was performed using threshold based analyses with customized Matlab (Mathworks Inc. Natick, MA, USA) routines incorporating principal component analysis of the spike waveform or

with the Matlab-based program SpikeTrain (Neurasmus BV, Erasmus MC Holding, Rotterdam, Netherlands).

GSWD-related firing pattern modulation

A custom-written algorithm in LabVIEW (National Instruments) was used to assess whether CN neurons showed GSWD-modulated firing patterns during GSWDs in the ECoG of the contralateral primary sensory cortex (in case of medial CN neurons) or primary motor cortex (in case of interposed or lateral CN neurons). The minimum total duration per episode was set at 2s to construct GSWD-triggered rasterplots and peri-GSWD-time-histograms (PSTH) with a 5-ms bin width, which allowed us to determine: 1) modulation amplitude: the amplitude difference between the peak and trough near t =0; 2) modulation frequency: frequency of the sine wave that fits the PSTH best; and 3) mean power at GSWD frequency: a Fast Fourier Transform between 6 and 9 Hz (GSWD frequency range). Next, the interspike intervals (ISIs) used for this PSTH were randomly shuffled 500 times and converted into a new PSTH with the same bin size to create normal distributions of modulation amplitude and mean power at GSWD frequency. Z-scores could now be calculated for the real and shuffled data by applying: $Z = (X-\mu)/\sigma$ where X =the value based on the original PSTH, μ =the mean of the bootstrapped normal distribution and σ =its standard deviation. Cells were identified as GSWD-modulated if: 1) the modulation amplitude should be significantly higher than expected by chance ($Z \geq 1.96$, $p \leq 0.05$); 2) the cell should modulate at GSWD frequency (6–9 Hz); and 3) The mean power at GSWD frequency should be significantly higher than expected by chance ($Z \geq 1.96$, $p \leq 0.05$). Since all CN neurons that showed significant Z-scores of mean power at GSWD frequency also showed significantly higher modulation amplitudes; the former was used for further analyses. The term Z-score refers to mean power at GSWD frequency unless stated otherwise.

Coherence

To determine the spectral coherence between the activity of a CN neuron and the ECoG signal during GSWDs, a custom-written Matlab (Mathworks) routine was used. The extracellular signal was time-binned at 1-ms precision, convolved with a sinc(x)-kernel (cut-off frequency =50 Hz) and down-sampled to 290 Hz. The ECoG signal was directly down-sampled to 290 Hz. The magnitude squared coherence was calculated per GSWD episode using Welch's averaged, modified periodogram method and is defined as: $C_{xy}(f) = \backslash P_{xy}(f) \backslash^2 / P_{xx}(f) * P_{yy}(f)$ with the following parameters: window = 290 (Hamming), noverlap = 75%, nfft = 290, sampling frequency = 290 (due to the window size only GSWDs > 1.5 s were considered). The coherence value per GSWD was defined as the maximum coherence in the 6–9 Hz frequency band; a weighted average per cell based on GSWD duration was used.

Firing pattern parameters

Firing patterns parameters were assessed using custom written LabVIEW (National Instruments) based programs calculating firing frequency, coefficient of variation (CV) of inter-spike intervals (ISIs) = σ_{ISI}/μ_{ISI}, CV2 = $2|ISI_{n+1} - ISI_n|/(ISI_{n+1} + ISI_n)$ and burst index = number of action potentials within bursts / total number of action potentials in a recording, where a burst is defined as ≥ 3 consecutive action potentials with an ISI ≤ 10 ms. CV reports regularity of firing throughout the whole recording and CV2 quantifies the regularity of firing on a spike-to-spike basis[38]. Firing pattern parameters were specifically calculated for ictal and interictal periods.

Regression analyses of inter-ictal CN activity

To evaluate whether there is a type of CN neuron that is predisposed for ictal phase-locking during GSWDs, we analyzed the neurons' interictal activity using a custom-made Matlab routine (Mathworks), aiming to probe the predictability of the ictal activity. We used Gaussian process regression[39], which is considered to be one of the best non-linear regression methods, to determine if the GSWD modulation of the activity was predictable from the interictal activity of the neurons. The measures that enabled the prediction of the modulation amplitude most accurately were CV, log-interval entropy, firing frequency and permutation entropy. The interictal parts of the extracellular recordings were divided into 1-s bins. To calculate the log-interval entropy, in which entropy measures the predictability of a system, first a natural logarithm of the intervals, in milliseconds, was taken to construct a histogram with a bin width of 0.02 log_e (time). Further, a Gaussian convolution was performed using a kernel of one-sixth SD of the log(ISIs). The entropy of the ISI histogram $p(I_i)$ was calculated by:

$$\mathrm{Ent}\,(\mathrm{I}) \;=\; -\sum_{i=1}^{N} \mathrm{p}\,(\mathrm{I_i}) \log_2 \mathrm{p}\,(\mathrm{I_i})$$

Furthermore, we analyzed the permutation entropy, which is calculated as the predictability of the order of neighboring ISIs rather than the actual values of the ISIs[40].

Normalized GSWD occurrence and duration

GSWDs were detected using the off-line ECoG detection algorithm described above. Total number of GSWDs and average GSWD duration were calculated and normalized to baseline values.

Assessment of cellular responses to optogenetic stimulation

Action potentials were detected as described above. A custom-written LabVIEW (National Instruments) program was used to construct light-triggered rasterplots and peri-stimulus-time-histograms with a 5-ms bin width. Changes in CN neuronal firing rate upon optical stimulation were subsequently determined by calculating the total number of action potentials during light pulses divided by the total

length of the pulse and compared with the baseline firing rate (calculated from the total recording time excluding the optogenetic stimulation). In the current study we consider differences in action potential firing rate exceeding 25% as responsive.

Assessment of impact of optogenetic stimulation of cerebellar output on GSWDs
The start and end of seizures were identified using the off-line GSWD detection method described above. A custom-written LabVIEW (National Instruments) program was used to assess the effectiveness of optogenetic stimulation in stopping GSWDs. Only light pulses triggered prior to the natural end of the seizure were used for analysis. The time difference between the light pulse and the end of the seizure was calculated. The seizure was considered 'stopped by the optogenetic stimulation' when this time difference did not exceed 150 ms. Mean power at GSWD frequency (6–9 Hz) was calculated using a Fast Fourier Transform of the ECoG signal recorded during 1-s or 0.5-s (in case of closed-loop optogenetic stimulation) time periods before and after the light pulse. Averaged responses to light pulses are represented per animal and per stimulus condition by averaging complex Morlet wavelets of 4-s windows ranging from 2 s before to 2 s after the stimulus.

Assessment of onset of optical cerebellar nuclei stimulation in relation to GSWD cycle
The time difference between the onset of stimulation and the last spike before stimulation was calculated and divided by the median length of one GSWD during that episode, representing one cycle of 360 degrees. The outcome was subsequently multiplied by 360. Note that the optogenetic stimuli were not initiated with a fixed delay after the occurrence of an ECoG-spike; the delay depended on the visual interpretation and reaction speed of the experimenter (for manual activation of the LED) or on the closed-loop detection system for which the delay depends on the variability of the ECoG directly prior to the GSWDs (see below and ref[41]).

Closed-loop GSWD detection
The GSWD detection system has been implemented using a real-time, digital wavelet-filter setup. The analog filter used for digitization has four functions: 1) amplification; 2) offset injection in order to match the signal to the input range of the Analog to Digital Converter (ADC); 3) artefact removal by using a second-order 0.4 Hz high-pass filter; and 4) antialiasing by means of a second-order 23.4 Hz low-pass filter. The filter is realized using discrete components on a prototype printed circuit board (PCB). Following the PCB the wavelet filter functionality is implemented on a TI Sitara AM335x ARM® microprocessor (Texas Instruments Inc. Dallas, TX, USA). It first digitizes the signal from the analog filter with its integrated ADC using a sampling frequency (fs) of 100 Hz. Subsequently the signal is filtered using a

wavelet filter and the GSWD episode is detected using signal thresholding. Upon detection an output LED is switched on to stimulate the target area in the cerebellum. Wavelet filters have previously been successfully applied for real-time GSWD detection[42]. Here we applied a complex Morlet wavelet at 6.7 Hz that resembled a GSWD. The wavelet filter was implemented as a Finite-Impulse-Response (FIR) filter by truncating the ideal complex Morlet as described earlier[43]. Using the two thresholds that are set manually during a recording session, the GSWDs are detected during a positive, high-threshold crossing and the detection is ended upon a negative, low-threshold crossing.

Statistical analyses

Statistical differences in firing pattern parameters between independent groups of CN neuronal recordings (*e.g.*, from *tg* mice, their wild-type littermates, GSWD-modulated and – non-modulated, pre- and post-gabazine injection) were determined using MANOVA's with firing frequency, CV, CV2 and burst index as dependent variables and group as independent variable. When a MANOVA showed a significant result, post-hoc ANOVA's were used to assess contributions of individual firing pattern parameters with Bonferroni corrected *p*-values.

Differences in coherence value between GWSD-modulated and -non-modulated cells were assessed using unpaired samples *t* tests. Cochran & Cox adjustment for the standard error of the estimate and the Satterthwaite adjustment for the degrees of freedom were used since equality of variances was not assumed.

Differences in normalized number of GSWD episodes and their duration between traces pre- and post-injection of either muscimol, gabazine or saline were tested by using non-parametric Friedman ANOVA's with one 'within-subjects' factor (*i.e.*, time period) with 2 levels (baseline and post injection).

Differences in mean power at 6–9 Hz before and after a light pulse were tested using values from all individual pulses by use of repeated measures ANCOVA's with one 'within-subjects' factor (*i.e.*, period) with 2 levels (pre and post light pulse) and 'mouse number' added as covariate to correct for variance in the within subjects factor explained by variance between mice. To test whether the time difference between the last ECoG-spike before optogenetic stimulation and the subsequent one deviates from the median interval between two ECoG-spikes in 'stopped seizures' a similar statistical approach was used. A repeated measures ANCOVA was used with one within subjects' factor with 2 levels, both time ECoG-spike intervals. Mouse number was again added as covariate. Since the number of seizures not terminated by the optogenetic stimulation was low, a non-parametric Friedman ANOVA was used to test the same difference.

To determine whether the phase angle of the optogenetic stimulation onset was related to the success rate of stopping GSWDs we compared the phase angle

distribution of successful attempts to that of the unsuccessful attempts. We tested for significant differences between these distributions using the non-parametric 2-sample Kuiper test.

A p-value ≤ 0.05 (α) was considered significant unless Bonferroni correction was used; in that case a p-value of α/n was considered significant. Two-tailed testing was used for all statistical analyses and all were performed using SPSS 20.0 software (IBM Corporation, New York, NY, USA). Exact information and outcomes regarding statistical testing are depicted in Tables 3.1–3.7.

3.3. RESULTS

3.3.1. GSWD related CN neuronal activity

We first investigated whether CN neuronal activity and ECoG were correlated during spontaneous episodes of GSWDs in awake head-fixed homozygous *tg* mice (Fig. 3.1A). We found no significant differences in GSWD occurrence ($t(24)$= −0.002, p = 0.998) and GSWD duration ($t(24)$ = 0.195, p = 0.847) between male and female *tg* mice, which is in line with data from other experimental animal models of absence epilepsy (reviewed by[44]). Therefore, we grouped data of both genders. GSWDs appeared simultaneously in bilateral primary motor (M1) and sensory cortices (S1) at 7.6 ± 0.6 Hz with an average duration of 3.6 ± 1.4s (N = 17 mice; Fig. 3.1B). The GSWD frequency and appearance were comparable to earlier reports of awake *tg* and other rodent models of absence epilepsy[30,32,34,45]. During these GSWDs, action potential firing of a subset of CN neurons was phase-locked to GSWDs. A typical GSWD-modulated CN neuron showed oscillatory action potential firing at GSWD frequency; repetitive firing was observed during the wave in the ECoG whereas the spike was accompanied by a pause in CN neuronal activity (Fig. 3.1C–E). These GSWD-modulated CN neurons showed significantly increased coherence with ECoG during seizures (p ≤ 0.001; Table 3.1). In each CN (MCN, IN and LCN) a substantial portion of the recorded CN neurons showed GSWD-modulated firing, with the highest percentage (73%; 49 out of 67 neurons) in the IN and 35% (35 out of 100 neurons) and 44% (19 out of 43 neurons) in the MCN and LCN respectively. We found no statistical difference (p = 0.512) in the phase of modulation of neuronal firing relative to the GSWD cycle for these three nuclei (Fig. 3.1D, F).

To assess whether GSWD-modulated CN neurons differed from non-modulating CN neurons in baseline activity, we compared their interictal firing patterns. During interictal periods GSWD-modulated CN neurons showed a higher firing frequency and a more irregular, burst-like firing pattern compared with non-modulated neurons (p-values < 0.01) and both modulated and non-modulated groups showed a more irregular firing pattern and increased burst index compared to CN

neurons recorded from wild-type littermates (*p*-values < 0.01; Fig. 3.1G; Table 3.1). Gaussian process regression[39] revealed that in *tg* mice interictal CN neuronal firing was correlated to the ictal firing pattern: 94% of neurons that phase-locked their activity to GSWDs could be predicted correctly, based on their interictal firing pattern (Fig. 3.1H). These data indicate that a large subset of neurons within each CN consistently shows seizure-modulated activity, *i.e.*, that these GSWD-modulated CN neurons are different from non-modulated neurons in basic, interictal firing patterns and that GSWD-related modulation can be predicted based on these interictal firing patterns.

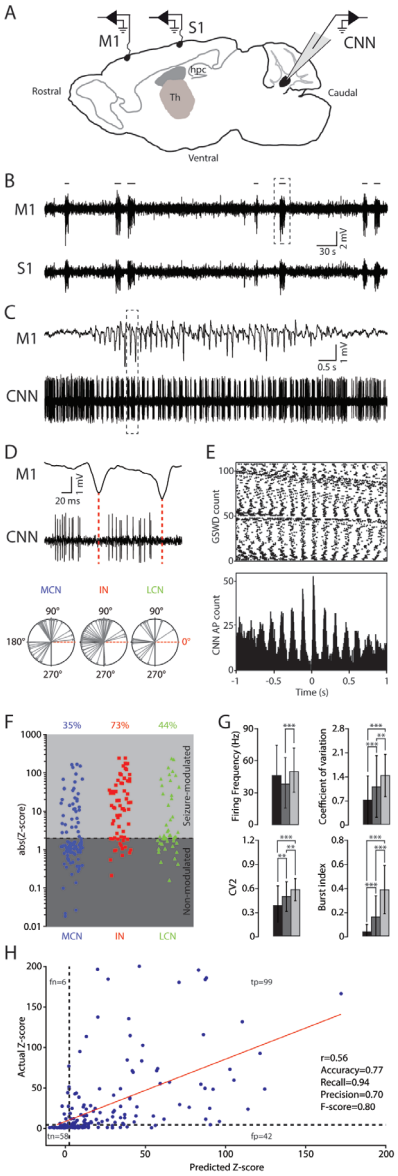

Fig. 3.1 *CN neuronal action potential firing patterns are modulated during GSWDs.*

(A) *Schematic of recording sites for ECoG from primary motor (MI) and sensory (SI) cortices and extracellular single-unit CN neuronal (CNN) recordings (Th = thalamus, Hpc = hippocampus).* ***(B)*** *ECoG from M1 and S1 with GSWD episodes (horizontal lines), indicating absence seizures.* ***(C)*** *Zoom of M1 episode outlined in panel B and simultaneously recorded action potential firing of a single CN neuron.* ***(D)*** *(top panel) Zoom of outlined M1 and CN neuronal recording in panel C. Red line aligns ECoG spike with pause in CN neuronal action potential firing. (bottom panel) Compass plot of phase difference between ECoG spike and modulated CN neuronal action potential firing.* ***(E)*** *Rasterplot and accompanying peri-SWD-time-*

*histogram of CN neuronal action potentials (AP) for three consecutive seizures (t = 0 is aligned with each ECoG spike). (**F**) Distribution of absolute Z-scores of mean power at GSWD frequency as determined by FFT for medial CN (MCN) interposed nuclei (IN) and lateral CN (LCN). Note that none of the negative Z-scores was below −1.96 and therefore showing absolute Z-scores does not change the number of data points below and above the l.96 cut-off score (corresponding to p < 0.05; horizontal dashed line). Total number recorded neurons: MCN n = 100; IN n = 67; LCN n = 43. (**G**) Barplots representing firing frequency, coefficient of variation, coefficient of variation 2 (CV2) and burst index for CN neurons recorded in wild-type littermate (n = 94; black) and seizure-modulated (n = 103; light grey) and non-modulated CN neurons recorded in tg (n = 107; dark grey). For clarity, we truncated the negative error bars. **p < 0.01, ***p < 0.001 (MANOVA, post-hoc ANOVA's with Bonferroni correction; see Table 3.l). (**H**) Result of the Gaussian process regression to predict the Z-score from interictal activity parameters (CV, firing frequency, log-interval entropy and permutation entropy) represented as a confusion matrix. The prediction is characterized as being a true positive (tp) when the predicted Z-score > 1.96 (dotted line) and the actual Z-score > 1.96. A true negative (tn) is scored when both predicted and actual Z-scores < 1.96. False positive (fp) and false negative (fn) refer to neurons which have been incorrectly predicted as "GSWD-modulated" and "GSWD-non-modulated", respectively. Note that we were able to achieve a precision of 0.70 and a recall of 0.94 which means that 70% of CN neurons (n = 210) that were predicted as "GSWD-modulated" were actually "GSWD-modulated" and 94% of all GSWD-modulated neurons has been identified correctly by the model. The Pearson correlation coefficient (r) between the predicted Z-score and the actual Z-score was 0.56 with p ≤ 0.05. **p < 0.01, ***p < 0.001.*

3.3.2. Impact on GSWD occurrence of pharmacological interventions that modulate CN action potential firing

CN neurons provide excitatory input to thalamic neurons[4,6,23–29] and thereby potentially contribute to the excitation-inhibition balance that sets thalamic activity patterns. Excess tonic inhibition of thalamic activity has been linked to the occurrence of absence seizures[3,7,8] and therefore we hypothesized that a decrease in CN output in *tg* should increase the occurrence of GSWDs, whereas increased CN output should have the opposite effect. To test this, we locally applied (Fig. 3.2A, Fig. 3.S1) either $GABA_A$-agonist muscimol, which stopped CN neuronal action potential firing (Fig. 3.2B) (no statistical comparison was possible due to complete cessation of action potential firing), or GABAA-antagonist gabazine (SR-95531), which consistently increased the frequency ($p < 0.01$) and regularity of CN neuronal firing ($p < 0.001$; Fig. 3.2B, C; Table 3.2). Upon bilateral CN injections with muscimol the occurrence of GSWDs increased by 160–3700% post-injection ($p < 0.01$; recorded for 60 min; peak of seizure occurrence 34.5 ± 16.5 min after injection; $N = 10$; Fig. 3.2D–F; Table 3.2). In contrast, bilateral CN injections with gabazine significantly reduced the occurrence of GSWDs ($p < 0.05$; first seizure occurred 32.5 ± 17.4 min after injection; $N = 10$) and bilateral sham injections did not change GSWD occurrence ($p = 0.18$) (Fig. 3.2D–F, H; Table 3.2). The duration of GSWDs was not significantly changed following muscimol, gabazine or saline injections in the CN (muscimol: $p = 0.21$; gabazine: $p = 0.32$; saline: $p = 0.41$; Fig. 3.2G; Table 3.2). As a control, we also injected similar quantities of gabazine or muscimol into the cerebellar cortex; this had no significant effect on the GSWD occurrence ($p = 0.66$ and 0.32 respectively)

or duration (p = 0.66 for both gabazine and muscimol injections) (Fig. 3.2H; Table 3.2). Thus, pharmacological manipulation of neuronal activity in the CN, but not the cerebellar cortex, is highly effective in modulating the occurrence of GSWDs in *tg* mice. Notably, we observed that muscimol and gabazine were most effective when the injections were in the IN and/or LCN (no statistical difference in impact on GSWD-occurrence after IN and/or LCN injections (p = 0.70; Mann Whitey U test) compared to injections in the MCN (p = 0.07 for muscimol and $p < 0.05$ for gabazine; Fig. 3.2F, G; Fig. 3.S1; Table 3.3). To study whether these differences in impact of pharmacological interventions aimed at the MCN or the IN and LCN were due to a variable effect on neuronal activity we also performed single-unit recordings in the injected CN. Regardless of the injected nucleus, muscimol effectively silenced all action potential firing and gabazine consistently increased the firing frequency and the regularity of action potential firing (all p-values < 0.01 for firing frequency, coefficient of variation and CV2; Table 3.4). These findings indicate that although effects of muscimol and gabazine on the neuronal activity were similar throughout all CN, the effect of manipulating activity in the IN and LCN seems to exert a larger impact on GSWD-occurrence than targeting the MCN. Pharmacological interventions in the CN of wild-type littermates (N = 2) did not evoke GSWD-episodes (data not shown).

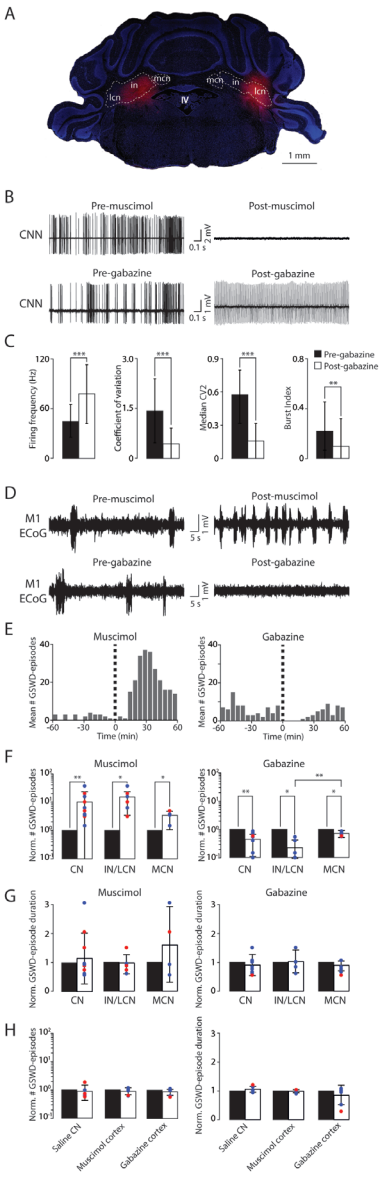

Fig. 3.2 *Bimodal modulation of GSWD occurrence by pharmacological manipulation of CN neuronal action potential firing.*

(***A***) *Confocal image of coronal cerebellar slice with bilateral muscimol injections (blue = DAPI; red = Evans blue indicating the injection sites; IV = 4th ventricle; MCN = medial CN; IN = interposed nucleus; LCN = lateral CN).* (***B***) *Examples of CN neuron (CNN) recordings before and after bilateral muscimol (top) and gabazine (bottom) injections.* (***C***) *Barplots for the impact of gabazine on CN neuronal firing as quantified by the difference between pre- and post-gabazine injections (n = 81 and n = 55, respectively) in fir-*

*ing frequency, coefficient of variation, median CV2 and burst index; **p < 0.01, ***p < 0.001 (MANOVA, post-hoc ANOVA's with Bonferroni corrections; see Table 3.2). (**D**) (top) Representative ECoG of primary motor cortex (Ml) ECoG pre- and post-muscimol injection and (bottom) representative M1 ECoG pre- and post-gabazine injection. (**E**) Time course of the effects of muscimol (left) and gabazine (right) on the average number of GSWD-episodes (bin-size = 5 minutes) (**F, G**) Normalized number of seizures (**F**) and normalized seizure duration (**G**) pre and post muscimol (left) and gabazine (right) injections (1 hr each) for bilateral injections in all CN (N = 10 for both gabazine and muscimol), in IN/LCN (N = 6 for muscimol and 5 for gabazine) and in MCN (N = 4 for muscimol and 5 for gabazine). Note that for quantification of the seizure duration post-gabazine injection, only 9 mice are included for the 'all CN' and 4 mice for the IN/LCN group, since one mouse did not show any GSWDs post-injection. Blue dots indicate data recorded from male mice and red dots from female.*p < 0.05, **p < 0.01, (Friedman's ANOVAs and Mann-Whitney U tests; see Tables 3.2 and 3.3). (**H**) Normalized number of GSWD-episodes (left) and normalized GSWD-episode duration (right) for control experiments; saline injections in the CN and muscimol and gabazine injections in superficial cerebellar cortical areas.*

Although it has been shown that pharmacological interventions can have sex-specific differences in animal models of epilepsy[46] that may contribute to the variability of the current results, our ECoG recordings did not show a trend towards a sex-specific impact of CN-specific muscimol or gabazine application (Fig. 3.2F–H). This finding was corroborated by the finding that muscimol was equally effective in stopping CN action potential firing in both male and female mice. Together, these effects indicate that in the *tg* animal model of absence epilepsy CN output forms an integral component of the neuronal networks involved in generalized epilepsy and may operate as a potent modulator of GSWD occurrence, irrespective of the gender.

3.3.3. Optogenetic stimulation of cerebellar nuclei

The promising impact of long-lasting pharmacological interventions at the level of the cerebellar output prompted us to explore whether short-lasting neuromodulation would be equally effective in stopping GSWDs, *i.e.*, whether disrupting oscillatory CN neuronal activity immediately stops GSWDs. To test this hypothesis we virally expressed light-sensitive channelrhodopsin-2 (ChR2) cation-channels in CN neurons (Fig. 3.3A). The optically-evoked alteration of CN neuronal firing (see below; Fig. 3.5A) had a robust effect on GSWD occurrence, in that most, if not all, episodes abruptly stopped within 150 ms of the onset of bilateral stimulation (N = 4; presented per mouse: 76% (male), 84% (female), 92% (female) and 100% (female) stopped) (Fig. 3.3B, C) and that the power at GSWD frequency was significantly reduced ($p < 0.001$) (Fig. 3.3F; Table 3.5). Moreover, unilateral optical stimulation of CN neurons proved equally effective in stopping GSWDs in all recorded cortices, regardless of the laterality (N = 3 female; presented per mouse: 89%, 92% and 100% stopped; power reduction: $p < 0.001$) (Fig. 3.3C, F; Table 3.5). Bilateral cerebellar stimulation was ineffective when a different wavelength (590 nm) was applied (N = 3 female; presented per mouse: 0%, 0% and 5% stopped; power reduction: $p = 0.37$) or when the optical fiber was placed outside the CN region (N = 3 female; presented

per mouse: 0%, 5% and 8% stopped; power reduction: $p = 0.28$) (Fig. 3.3D, F; Table 3.5).

The type of seizure detection and on-demand stimulation described above renders the procedure conceptually unsuitable for clinical implementation in that it would require constant on-line evaluation and decision-making by medics[47]. Therefore, we developed a brain-machine-interface (BMI) approach by engineering a closed-loop system for online detection of GSWDs and subsequent optogenetic stimulation[41]. Using off-line analysis we optimized the performance of a wavelet-based GSWD detection filter up to an accuracy of 96.5% and a median latency of 424 ms. When applied online this on-demand, closed-loop stimulation proved efficient in detecting and stopping GSWDs; bilateral optical stimulation of ChR2-expressing CN neurons stopped 93.4% of GSWDs and unilateral stimulation stopped 91.8% of GSWDs, which is also represented by the GSWD frequency power reduction ($N = 3$ female; $p < 0.001$; Fig. 3.3E, 3.3F; Table 3.5). Together, these data highlight that also in a clinically applicable BMI setting single-pulse stimulation of CN neurons suffices to stop GSWDs and that unilateral stimulation is sufficiently powerful to disrupt bilateral thalamocortical oscillations.

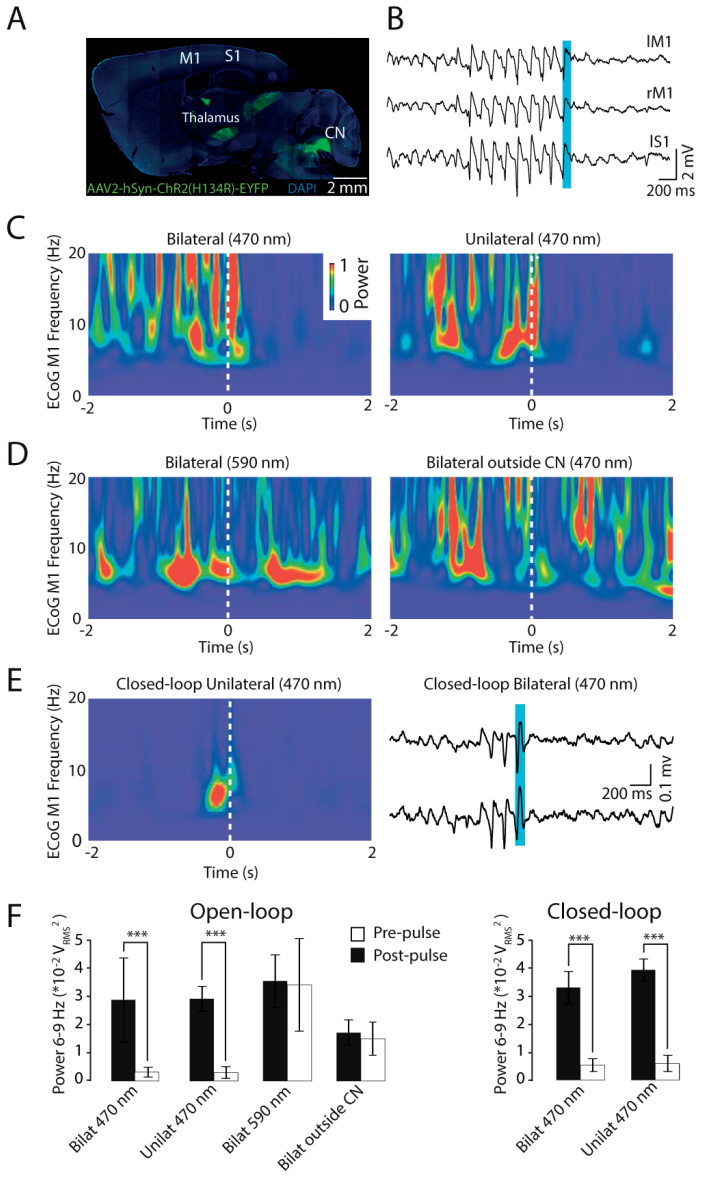

Fig. 3.3 *Optogenetic stimulation of cerebellar nuclei reliably stops GSWDs.*

*(**A**) Confocal image of sagittal brain section showing ChR2-expression in cerebellar nuclei (CN) with projections to the thalamus (Th) (MI, SI represent primary motor and sensory cortex respectively). (**B**) Representative ECoG of bilateral M1 (left (l) and right (r) M1) and left SI recording (lSI) which exemplifies how bilateral optogenetic stimulation (470 nm light pulse of l00 ms indicated by the vertical blue bar) stops GSWDs in all recorded cortices. (**C**) Mean ECoG wavelet spectrogram of contralateral M1 for all bilateral (n = 25; left panel) and unilateral stimuli (n = 11; right panel) presented to a single mouse at 470 nm. (**D**) As in panel d for (left) 590 nm stimuli (n = 36) and stimulation at 470 nm outside of CN (right) (n =*

*18). (**E**) (Right panel) Typical example of the effect of bilateral closed-loop stimulation on GSWD recorded in contralateral M1 and S1 and (left panel) mean ECoG wavelet spectrogram of all unilateral stimuli (n = 44) presented to one mouse. (**F**) ECoG theta-band power before and after open-loop (bilateral N = 4; n = 178); unilateral N = 3; n = 43), stimulations with the wrong wavelength (590 nm) (N = 3; n = 107) and stimulations outside the CN (N = 3; n = 185) as well as the responses to closed-loop stimulation at 470 nm in the CN (bilateral N = 3; n = 227; unilateralN = 3; n = 49). ***p < 0.001 (repeated-measures ANCOVA; see Table 3.5).*

3.3.4. Key findings are replicated in an unrelated mouse model of absence epilepsy

To exclude the possibility that our current findings in *tg* are unique to their pathophysiology[30, 48, 49], we repeated key experiments in *C3H/HeOuJ*, an inbred strain with an absence epilepsy phenotype[33] that is unrelated to *tg*. Extracellular recordings in awake ECoG-monitored *C3H/HeOuJ* mice confirmed that a smaller but substantial portion (35%) of CN neurons showed phase-locked action potential firing (Fig. 3.4A, B) and significant coherence with ECoG ($p < 0.001$; Table 3.6) during GSWDs and that this oscillatory firing was more irregular than their interictal firing pattern ($p < 0.001$; Fig. 3.4C; Table 3.6).

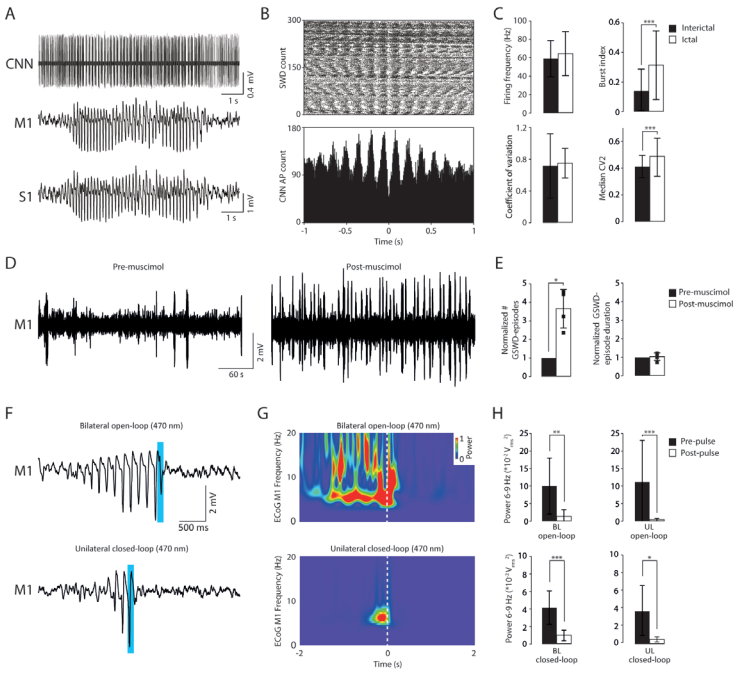

Fig. 3.4 *Modulation of phase-locked CN neuronal activity stops GSWDs in C3H/HeOuJ mice.*

*(**A**) Simultaneously recorded primary motor (M1) and sensory (S1) cortex ECoGs and CN neuronal activity. (**B**) Rasterplot and peri-stimulus time histogram of single CN neuronal activity (t = 0 indicates each ECoG spike). (**C**) Summary barplots representing the mean differences in firing pattern parameters between*

*interictal and ictalperiods (n = 28). ***p < 0.001 (repeated-measures ANOVA with Bonferroni corrections; see Table 3.6). (**D**) Representative M1 ECoG of pre- and post-muscimol injection and (**E**) corresponding normalized seizure occurrence and duration. *p < 0.05 (Friedman's ANOVA; see Table 3.6). (**F-H**) Open- (top) and closed-loop (bottom) optogenetic stimulation stops GSWDs as shown by: (**F**) typical example trace; by (**G**) ECoG wavelet spectrogram averaged over all bilateral open-loop (n = 11; top panel) stimuli in a single mouse and over all unilateral closed-loop stimuli (n = 18; bottom panel) in another mouse; and by (**H**) ECoG theta-band power before and after optical stimulation for bilateral open-loop stimuli (N = 3, n = 19; top left panel), unilateral open-loop stimuli (N = 3, n = 19), bilateral closed-loop stimuli (N = 3, n = 46) and unilateral closed-loop stimuli (N = 3, n = 30). ***p < 0.001 (repeated-measures ANCOVA; see Table 3.6).*

Similar to *tg* mutants (Fig. 3.2), *C3H/HeOuJ* mice showed significantly more seizures following local muscimol injections into CN ($p < 0.05$; Fig. 3.4D, E; Table 3.6). Moreover, also in *C3H/HeOuJ* optogenetic stimulation reliably stopped GSWD-episodes ($N = 3$; presented per mouse: 82%, 87% and 91% stopped) and both bilateral and unilateral stimuli significantly reduced power at GSWD frequency ($p < 0.01$ and $p < 0.001$, respectively); the closed-loop detection and intervention system reduced the GSWD frequency power ($p < 0.001$ for bilateral and $p < 0.05$ for unilateral stimulation); and neither optical stimulation at 590 nm nor stimulation outside of CN significantly reduced the GSWD frequency power ($p = 0.43$ and $p = 0.81$, respectively; Fig. 3.4H; Table 3.6). Thus, the main findings done on CN treatment of absence seizures in *tg*, could be replicated in *C3H/HeOuJ* mutants.

3.3.5. Optogenetic stimulation of presumptively excitatory CN neurons affects GSWDs

To investigate the mechanism underlying the potent interruption of GSWDs by optogenetic stimulation of CN in *tg* and *C3H/HeOuJ*, we quantified the responses of CN neurons to bilateral optical stimulation. In *C3H/HeOuJ* and *tg* injected with AAV2-hSyn-ChR2 (H134R)-EYFP 33 out of 50 responsive cells (66%) showed increased action potential firing, whereas 17 (34%) showed decreased firing (Fig. 3.5A). A further 16 recorded neurons showed no response to optical stimulation. This variety of responses is in line with the properties of the construct that was used to transfect CN neurons with ChR2. Since human synapsin (hSyn) is not specific to a certain type of CN neuron[50] both excitatory and inhibitory neurons expressed ChR2. Excitatory responses can be recorded from neurons that express ChR2, inhibitory responses can be recorded from neurons that do not express ChR2 but that receive input from ChR2-positive inhibitory neurons, while neurons devoid of ChR2 expression either in their membrane or synaptic afferents will not show any response.

Next, we questioned to what extent the impact of optogenetic stimulation of CN neuronal action potential firing depends on the phase of the thalamocortical oscillations, *i.e.*, to what extent the disruption of GSWD-modulated CN firing was evoked during cortical excitation (the ECoG spike) and/or cortical inhibition (the ECoG wave)[51]. Since we did not design our stimulation protocol to be activated with a fixed delay relative to the GSWDs, we could answer this question by comparing

the phase values of the onset of effective stimuli relative to the Spike-and-Wave cycle in M1 and S1 cortices with those of ineffective stimuli (Fig. 3.5B). For both M1 and S1 success rates were lowest when the stimulus was applied up to 60 degrees before the peak of a spike (i.e., 300°–360° in Fig. 3.5C lower panels), but the overall differences of these distributions did not reach statistical significance (M1: $p = 0.13$; S1: $p = 0.29$). However, effective stimuli evoked a significant shortening ($p < 0.01$) of the interval between the last two ECoG-spikes, which is indicative of an excitatory effect on cortical activity[51] (Fig. 3.5D; Table 3.7), and the timing of the last ECoG-spike could be predicted by the time of the stimulus onset relative to the spike-and-wave-discharge cycle ($p < 0.001$; Fig. 3.5E; Table 3.7). Together, our combined electrophysiological and optogenetic data indicate that optogenetic CN stimulation is most effective when applied during the 'wave' of the GSWD, during which cortical neurons are normally silent.

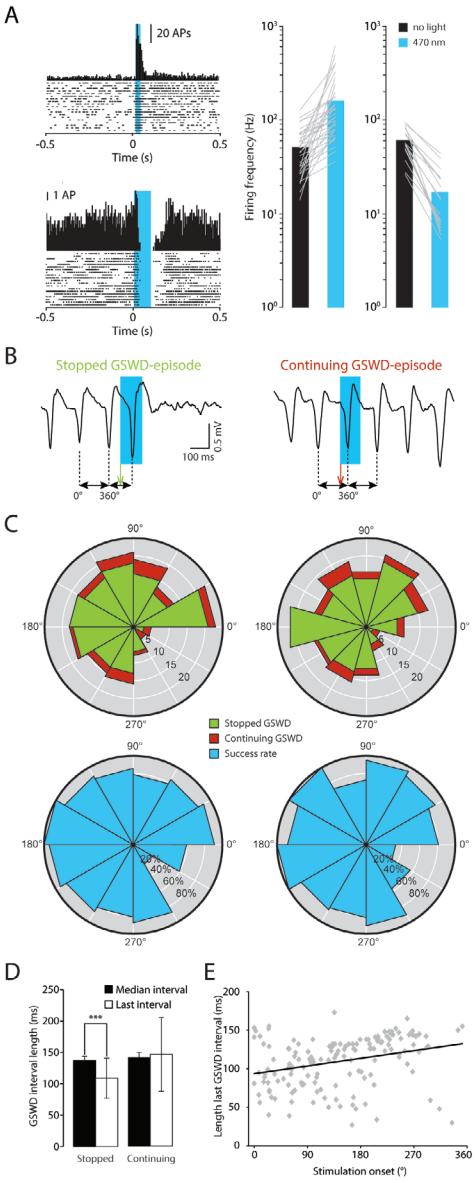

Figure 3.5 Excitatory impact of optical CN stimulation on cortical activity stops GSWD-episodes

(**A**) (Left panels) Peri-stimulus time histogram and rasterplot indicating increased (top) or decreased (bottom) action potential (AP) firing for individual CN neurons evoked by 470 nm light pulses (blue bars). (Right panels) Scatterplots represent the individual changes in CN neuronal firing following optical stimulation: (left) increased firing (n = 33); (right) decreased firing n = 17). Black and blue bars indicate mean firing frequency when the 470 nm LED was turned off or on, respectively (**B**) Examples

of stopped (left) and continuing (right) GSWD episodes upon optogenetic stimulation. Black horizontal arrows represent the median time interval between ECoG 'spikes', which correspond to one cycle of cortical oscillation, here represented as 360 degrees. Green and red vertical arrows represent the onset of the light stimulus. (**C**) Rose plots of the start of successful and unsuccessful optical stimulation in the 360° GSWD cycle for both primary motor cortex (M1; left) and primary sensory cortex (S1; right). (**D**) Comparison between the median and the last interval (between the last two ECoG-spikes) for stopped and continuing GSWD episodes. ***$p < 0.001$ (repeated measures ANCOVA; see Table 3.7). (**E**) Scatterplot representing the predictability of the stimulus-related time interval between GSWDs by the phase of stimulation-onset ($p < 0.001$; linear regression analysis; see Table 3.7).

3.4. DISCUSSION

In this study we show that in two unrelated mouse models of absence epilepsy the activity of CN neurons can be utilized to modulate the occurrence of GSWDs. We provide evidence that pharmacological interventions at the level of CN can exert slow, but long-term, effects and that optogenetic stimulation of CN neurons can exert fast, short-term control. The different dynamics of these experimental approaches, with converging outcomes, align with the hypothesis that CN neurons can control the balance of excitation and inhibition in the thalamus, thereby resetting the oscillatory activity in thalamocortical loops. In both *tg* and *C3H/HeOuJ* strains of mice a substantial subset of CN neurons showed phase-locked action potential firing during GSWDs, which is in line with a previous study of oscillating cerebellar activity during GSWDs in WAG/Rij and F344/BN rats[32]. We observed that 35% of neuronal recordings in the MCN showed GSWD-modulated patterns, whereas the portions of GSWD-modulated neurons in the IN and LCN were higher (73% and 44%, respectively). Except for an anatomical evaluation of the local density of large and small soma-diameter CN neurons in the mouse brain[52] and computational studies on the clustering analysis of CN neuronal action potential firing in *tg*[53,54], little experimental data are available that allow us to unequivocally pinpoint the type (s) of CN neurons responsible for modification of GSWD activity. With respect to the extracellular recordings we presumably recorded mostly from CN neurons with a large soma-diameter[55], which incorporates mainly excitatory glutamatergic neurons[56], but in the MCN also inhibitory glycinergic projection neurons[57]. Interestingly, GSWD-modulated CN neurons also showed characteristic firing patterns during the periods in between the seizures. During these interictal periods they fired at higher frequencies with a more irregular and burst-like pattern than the CN neurons that did not co-modulate with GSWDs. Thus, the interictal firing pattern of CN neurons in *tg* and *C3H/HeOuJ* mice appears to reliably predict whether these cells will show oscillations phase-locked to GSWDs during seizures.

Pharmacological manipulation of neuronal activity in the cerebellum proved effective when the injections of muscimol or gabazine were aimed at the CN, but not when the cerebellar cortex was targeted. We found that gabazine application

was effective in reducing GSWD occurrence in all CN with the most pronounced effects in IN and LCN. Along the same line, muscimol injections in IN and LCN evoked the biggest increase in GSWD occurrence. Effects of MCN injections were smaller but still significant. Since we know little about the density of individual types of neurons throughout the murine MCN, IN and LCN[52,56], and considering the similarity in effects of gabazine and muscimol on neuronal activity in these nuclei, we cannot draw a firm conclusion about a potentially differential effect of either gabazine or muscimol on the respective nuclei. These data raise the possibility that the difference in impact on GSWD occurrence between manipulation of MCN vs. that of IN and LCN does not reflect a difference in intrinsic activity, but rather a difference in their efferent projections to the brainstem, midbrain and thalamus[24]. Although all CN have been shown to project to a wide range of thalamic subnuclei, like the ventrolateral, ventromedian, centrolateral, centromedian and parafascicular nuclei[24, 58] and thereby connect to a variety of thalamocortical networks, the impact of IN and LCN has been shown to focus on the primary motor cortex whereas MCN impacts more diffusely on thalamocortical networks[59].

CN axons that project to the thalamus have been shown to originate from glutamatergic neurons, which synapse predominantly perisomatically and evoke substantial excitatory responses[4, 6, 23–29]. Upon CN injections with muscimol, we must in effect have substantially reduced the level of excitation of thalamic neurons and thereby disturbed the balance of inhibition and excitation in thalamocortical networks in favor of inhibition. One of the main consequences of hyperpolarizing the membrane potential of thalamic neurons through this inhibition is activation of hyperpolarization-activated depolarizing cation currents (I_h) and $Ca_V3.1$ (T-type) Ca^{2+}-currents, which typically results in the burst-like action potential firing that can drive GSWDs in thalamocortical networks[7, 8, 60, 61]. Moreover, in *tg* thalamic relay neurons show increased T-type Ca^{2+} channel currents[62], which probably act synergistically with the decreased excitation following muscimol treatment, likely further increasing GSWD occurrence. In contrast, when we applied gabazine to CN, the balance of inhibition and excitation in the thalamocortical networks probably shifted towards excitation and thereby may have prevented the activation of I_h and T-type Ca^2+-channel currents, reducing the occurrence of burst firing and GSWDs. The successful application of short periods of optogenetic excitation of CN neurons did not only confirm the de-oscillating impact of gabazine, but further refined it by revealing that GSWDs can be most efficiently stopped when the interval between ECoG spikes, *i.e.*, wavelength of the oscillations, is instantly shortened and thereby reset. Given the relatively low success rate of optogenetic stimulation in the period just preceding the 'Spike' state of the GSWDs, which reflects the excitation state of the thalamocortical relay neurons, it is parsimonious to explain the effective resetting through optimal interference during the inhibitory or 'Wave' state of the

GSWD[51]. This explanation centered on the resetting hypothesis argues against the possibility that GSWDs were terminated by optogenetic activation of the CN neurons that were inhibited. Regardless of the *netto* effect of CN stimulation on thalamocortical networks, the current approach proved equally effective when applied bilateral or unilateral. Most likely, instantly resetting the balance of excitation and inhibition in thalamocortical relay neurons on one side of the brain will also engage the other side through combined ipsi- and contralateral projections from the CN to the thalamus and through interthalamic and intercortical connections[6, 24, 63].

It remains to be established to what extent the current findings for absence epilepsy can help to treat epileptic patients suffering from other types of seizures. Our findings on the impact of optogenetic manipulation of CN firing patterns on GSWD occurrence seem to support that (pre-)clinical studies that apply DBS[64, 65] in the CN may be an option to treat epilepsy patients. So far, only three clinical studies applying electrical deep brain stimulation (DBS) to the CN have been reported, which is in contrast to the dozens of studies performed to investigate the therapeutic use of cerebellar surface stimulation (as reviewed by ref[66]). Although initially promising, the clinical studies on the effects of cerebellar surface stimulation reported inconsistent results[12–21], which may partially be due to suboptimal placement of electrodes. Unlike the current results, which show a regional preference for the effect of lateral CN stimulation on GSWD occurrence, it was recently shown that manipulating Purkinje cells in the medial cerebellum is most effective in controlling kainate-induced temporal lobe epilepsy[67]. So far, the studies that applied DBS at the level of CN in an uncontrolled fashion report highly effective decreases in the level of seizures (corresponding to class IC and IIIA of the Engel scale[68]) in a low number of patients characterized with various types of epilepsy[69–71]. Apart from the coherence in location of stimulation (laterally located nucleus dentatus) these studies used a wide variety in CN stimulus regimes, ranging from 3 min per day to continuous electrical stimulation for 12–14 hrs per day. It appears that high-frequency stimulation (> 50 Hz), but not low-frequency stimulation (1–40 Hz), is most effective when applied to the cerebellar dentate nucleus. In the present study we found that the increase in CN neuronal action potential firing frequency upon optogenetic stimulation was highly variable (Fig. 3.5) and thus our current results do not provide any ground for a conclusion on whether low- or high-frequency stimulation would be advantageous to stop GSWD-episodes. Yet, our results do provide sufficient data to conclude that the temporal precision determines the level of efficiency, e.g., by stimulating with short pulses as soon as an epileptic event starts to occur and if possible in a proper temporal relation with respect to the inhibitory wave of the GSWDs.

Since absence epilepsy is a commonly prevalent but in essence a benign form of generalized epilepsy[1], DBS will not very likely be considered as a serious option.

However, patients diagnosed with other forms of epilepsy whom do not benefit sufficiently from medication, may be eligible for (cerebellar) DBS[47]. Currently, the options for applying DBS are (too) limited; only the anterior thalamic nucleus is currently described in the FDA-guidelines to treat intractable epilepsy, and although promising, the outcome is limited and can result in cognitive and emotional problems[72, 73]. Given the powerful impact of CN stimulation on thalamocortical activity that is shown in the present study, we hypothesize that CN stimulation may also exert very positive effects in these other, more severe kinds of epilepsies.

ACKNOWLEDGEMENTS:

Support was provided by the Netherlands Organization for Scientific Research (NWO)-ALW, MAGW, ZON-MW (A.M.J.M.v.d.M, C.I.D.Z and F.E.H.), EU "EUROHEADPAIN" grant (nr 602633) (A.M.J.M.v.d.M), an LUMC Fellowship (E.A.T.), Marie Curie Career Integration Grant (nr 294233) (E.A.T.), the Centre for Medical Systems Biology (CMSB) in the framework of the Netherlands Genomics Initiative (NGI) (A.M.J.M.v.d.M.), Neuro-Basic, ERC-advanced and ERC-POC (C.I.D.Z.), NWO-VENI, NWO-VIDI and EUR-Fellowship (F.E.H.). We thank Dr. Karl Deisseroth for providing the AAV-hSyn-ChR2 (Hl34R)-EYFP and we thank Drs. T.J. Ruigrok, L. Bosman and P. Holland, K. Voges, R. Seepers, E. Haasdijk, E. Goedknegt, M. Rutteman, D. Groeneweg and P. Plak for technical assistance and/or constructive discussions.

3.5. REFERENCES

1. Berg, A.T., et al. Revised terminology and concepts for organization of seizures and epilepsies: Report of the ILAE Commission on Classification and Terminology, 2005–2009. *Epilepsia* 51, 676–685 (2010).
2. Jallon, P., Loiseau, P. & Loiseau, J. Newly diagnosed unprovoked epileptic seizures: presentation at diagnosis in CAROLE study. Coordination Active du Reseau Observatoire Longitudinal de l'Epilepsie. *Epilepsia* 42, 464–475 (2001).
3. Snead, O.C., 3rd. Basic mechanisms of generalized absence seizures. *Ann. Neurol.* 37, 146–157 (1995).
4. Norden, A.D. & Blumenfeld, H. The role of subcortical structures in epilepsy. *Epilepsy Behav.* 3, 219–231 (2002).
5. Paz, J.T., et al. A new mode of corticothalamic transmission revealed in the Gria4(-/-) model of absence epilepsy. *Nat. Neurosci.* 14, 1167–1173 (2011).
6. Jones, E.G. The Thalamus 2nd Edition. (Cambridge University Press, New York, 2007).
7. Blumenfeld, H. & McCormick, D.A. Corticothalamic inputs control the pattern of activity generated in thalamocortical networks. *J. Neurosci.* 20, 5153–5162 (2000).

8. Cope, D.W., et al. Enhanced tonic GABAA inhibition in typical absence epilepsy. *Nat. Med*. 15, 1392–1398 (2009).
9. Huguenard, J.R. & McCormick, D.A. Thalamic synchrony and dynamic regulation of global forebrain oscillations. *Trends Neurosci*. 30, 350–356 (2007).
10. Paz, J.T., et al. Closed-loop optogenetic control of thalamus as a tool for interrupting seizures after cortical injury. *Nat. Neurosci*. 16, 64–70 (2013).
11. Berenyi, A., Belluscio, M., Mao, D. & Buzsaki, G. Closed-loop control of epilepsy by transcranial electrical stimulation. *Science* 337, 735–737 (2012).
12. Cooper, I.S. Effect of chronic stimulation of anterior cerebellum on neurological disease. *Lancet* 1, 206 (1973).
13. Cooper, I.S., Amin, I., Riklan, M., Waltz, J.M. & Poon, T.P Chronic cerebellar stimultion in epilepsy. Clinical and anatomical studies. *Arch. Neurol*. 33, 559–570 (1976).
14. Cooper, I.S., Riklan, M., Watkins, S. & McLellan, D. Safety and efficacy of chronic stimulation. *Neurosurgery* 1, 203–205 (1977).
15. Dow, R.S., Smith, W. & Maukonen, L. Clinical experience with chronic cerebellar stimulation in epilepsy and cerebral palsy. *Electroencephalogr. Clin. Neurophysiol*. 43, 906 (1977).
16. Gilman, S., et al. Clinical, morphological, biochemical, and physiological effects of cerebellar stimulation. in *Functional Electrical Stimulation: Applications in Neural Prosthesis* (Marcel Dekker, New York, 1977).
17. Levy, L.F. & Auchterlonie, W.C. Chronic cerebellar stimulation in the treatment of epilepsy. *Epilepsia* 20, 235–245 (1979).
18. Bidziński, J., Bacia, T., Ostrowski, K. & Czarkwiani, L. Effect of cerebellar cortical electrostimulation on the frequency of epileptic seizures in severe forms of epilepsy. *Neurol. Neurochir. Pol*. 15, 605–609 (1981).
19. Wright, G.D., McLellan, D. & Brice, J.G A double-blind trial of chronic cerebellar stimulation in twelve patients with severe epilepsy. *J. Neurol. Neurosurg. Psych*. 47, 769–774 (1984).
20. Van Buren, J.M., Wood, J.H., Oakley, J. & Hambrecht, F. Preliminary evaluation of cerebellar stimulation by double-blind stimulation and biological criteria in the treatment of epilepsy. *J. Neurosurg*. 48 (1978).
21. Velasco, F., et al. Double-blind, randomized controlled pilot study of bilateral cerebellar stimulation for treatment of intractable motor seizures. *Epilepsia* 46, 1071–1081 (2005).
22. De Zeeuw, C.I., et al. Spatiotemporal firing patterns in the cerebellum. *Nat. Rev. Neurosci*. 12, 327–344 (2011).
23. Aumann, T.D. & Horne, M.K. Ramification and termination of single axons in the cerebellothalamic pathway of the rat. *J. Comp. Neurol*. 376, 420–430 (1996).
24. Teune, T.M., Van der Burg, J., Van der Moer, J. & Ruigrok, T.J. Topography of cerebellar nuclear projections to the brain stem in the rat. *Prog. Brain Res*. 124, 141–172 (2000).

25. Sawyer, S.F., Tepper, J.M. & Groves, P.M Cerebellar-responsive neurons in the thalamic ventroanterior-ventrolateral complex of rats: light and electron microscopy. *Neuroscience* 63, 725–745 (1994).
26. Sawyer, S.F., Young, S.J., Groves, P.M. & Tepper, J.M Cerebellar-responsive neurons in the thalamic ventroanterior-ventrolateral complex of rats: in vivo electrophysiology. *Neuroscience* 63, 711–724 (1994).
27. Uno, M., Yoshida, M. & Hirota, I. The mode of cerebello-thalamic relay transmission investigated with intracellular recording from cells of the ventrolateral nucleus of cat's thalamus. *Exp. Brain Res*. 10, 121-139 (1970).
28. Shinoda, Y., Futami, T. & Kano, M. Synaptic organization of the cerebello-thalamocerebral pathway in the cat. II. Input-output organization of single thalamocortical neurons in the ventrolateral thalamus. *Neuroscience research* 2, 157–180 (1985).
29. Bava, A., Manzoni, T. & Urbano, A. Effects of fastiginal stimulation on thalamic neurones belonging to the diffuse projection system. *Brain research* 4, 378–380 (1967).
30. Noebels, J.L. & Sidman, R.L. Spike-Wave and focal motor seizures in the mutant mouse tottering. *Science* 204, 1334–1336 (1979).
31. Fletcher, C.F., et al. Absence epilepsy in tottering mutant mice is associated with calcium channel defects. *Cell* 87, 607–617 (1996).
32. Kandel, A. & Buzsaki, G. Cerebellar neuronal activity correlates with spike and wave EEG patterns in the rat. *Epilepsy Res*. 16, 1–9 (1993).
33. Tokuda, S., Beyer, B.J. & Frankel, W.N Genetic complexity of absence seizures in substrains of C3H mice. *Genes Brain Behav*. 8, 283–289 (2009).
34. Marescaux, C., Vergnes, M. & Depaulis, A. Genetic absence epilepsy in rats from Strasbourg-a review. *J. Neural Transm. Suppl*. 35, 37–69 (1992).
35. Kaplan, B.J., Seyfried, T.N. & Glaser, G.H Spontaneous polyspike discharges in an epileptic mutant mouse (tottering). *Exp Neurol* 66, 577–586 (1979).
36. Hoebeek, F.E., Witter, L., Ruigrok, T.J. & De Zeeuw, C.I. Differential olivo-cerebellar cortical control of rebound activity in the cerebellar nuclei. *Proc. Natl. Acad. Sci. U.S.A*. 107, 8410–8415 (2010).
37. Loureiro, M., et al. The ventral midline thalamus (reuniens and rhomboid nuclei) contributes to the persistence of spatial memory in rats. *J. Neurosci*. 32, 9947–9959 (2012).
38. Holt, G.R., Softky, W.R., Koch, C. & Douglas, R.J Comparison of discharge variability in vitro and in vivo in cat visual cortex neurons. *J. Neurophys*. 75, 1806–1814 (1996).
39. Rasmussen, C.E. & Williams, C.K.I. Gaussian processes for machine learning. (The MIT Press, Cambridge, MA, U.S.A., 2006).
40. Bandt, C. & Pompe, B. Permutation entropy: a natural complexity measure for time series. *Phys. Rev. Lett*. 88, 174102 (2002).
41. van Dongen, M.N., et al. An implementation of a wavelet-based seizure detection filter suitable for realtime closed-loop epileptic seizure suppression. in *IEEE Biomedical Circuits and Systems Conference (BioCAS 2014)* (Lausanne, Switzerland, 2014).

42. Osorio, I., Frei, M.G. & Wilkinson, S.B Real-time automated detection and quantitative analysis of seizures and short-term prediction of clinical onset. *Epilepsia* 39, 615–627 (1998).
43. Karel, J.M.H., et al. Implementing wavelets in continuous-time analog circuits with dynamic range optimization. *IEEE Transactions on Circuits and Systems – I* 59, 229–242 (2012).
44. van Luijtelaar, G., Onat, F.Y. & Gallagher, M.J. Animal models of absence epilepsies: What do they model and do sex and sex hormones matter? *Neurobiology of disease* 72PB, 167–179 (2014).
45. van Luijtelaar, G. & Zobeiri, M. Progress and outlooks in a genetic absence epilepsy model (WAG/Rij). *Current medicinal chemistry* 21, 704–721 (2014).
46. Akman O., Moshe S.L., Galanopoulou A.S. Sex-specific consequences of early life seizures. *Neurobiology of disease*. 72 Pt B, 153–66 (2014).
47. Fisher, R.S. & Velasco, A.L. Electrical brain stimulation for epilepsy. *Nat. Rev. Neurol*. 10, 261–270 (2014).
48. Hoebeek, F.E., Khosrovani, S., Witter, L. & De Zeeuw, C.I. Purkinje cell input to cerebellar nuclei in tottering: ultrastructure and physiology. *Cerebellum* 7, 547–558 (2008).
49. Hoebeek, F.E., et al. Increased noise level of purkinje cell activities minimizes impact of their modulation during sensorimotor control. *Neuron* 45, 953–965 (2005).
50. Nathanson, J.L., Yanagawa, Y., Obata, K. & Callaway, E.M Preferential labeling of inhibitory and excitatory cortical neurons by endogenous tropism of adeno-associated virus and lentivirus vectors. *Neuroscience* 161, 441–450 (2009).
51. Polack, P.O. & Charpier, S. Intracellular activity of cortical and thalamic neurones during high-voltage rhythmic spike discharge in Long-Evans rats in vivo. *J. Physiol*. 571, 461–476 (2006).
52. Heckroth, J.A. Quantitative morphological analysis of the cerebellar nuclei in normal and lurcher mutant mice. I. Morphology and cell number. *J. Comp. Neurol*. 343, 173–182 (1994).
53. Alva, P., et al. Combining manchine learning and simulations of a morphologically realistic model to study modulation of neuronal activity in cerebellar nuclei during absence epilepsy. *BMC Neuroscience* 15 (Suppl 1), P39 (2014).
54. Alva, P., et al. A potential role for the cerebellar nuclei in absence seizures. *BMC Neuroscience* 14, 170 (2013).
55. Rowland, N.C. & Jaeger, D. Coding of tactile response properties in the rat deep cerebellar nuclei. *J Neurophysiol* 94, 1236–1251 (2005).
56. Uusisaari, M. & Knopfel, T. Functional classification of neurons in the mouse lateral cerebellar nuclei. *Cerebellum* 10, 637–646 (2011).
57. Bagnall, M.W., et al. Glycinergic projection neurons of the cerebellum. *J Neurosci* 29, 10104–10110 (2009).
58. Aumann, T.D., Rawson, J.A., Finkelstein, D.I. & Horne, M.K Projections from the lateral and interposed cerebellar nuclei to the thalamus of the rat: a light and electron

microscopic study using single and double anterograde labelling. *J Comp Neurol* 349, 165–181 (1994).
59. Steriade, M. Two channels in the cerebellothalamocortical system. *J Comp Neurol* 354, 57–70 (1995).
60. Andersen, P., Eccles, J.C. & Sears, T.A The ventro-basal complex of the thalamus: types of cells, their responses and their functional organization. *J. Physiol.* 174, 370–399 (1964).
61. Destexhe, A., Contreras, D. & Steriade, M. Mechanisms underlying the synchronizing of corticothalamic feedback through inhibition of thalamic relay cells. *J. Neurophysiol.* 79, 999–1016 (1998).
62. Zhang, Y., Mori, M., Burgess, D.L. & Noebels, J.L Mutations in high-voltage-activated calcium channel genes stimulate low-voltage-activated currents in mouse thalamic relay neurons. *J Neurosci* 22, 6362–6371 (2002).
63. Chan-Palay, V. *Cerebellar Dentate Nucleus: Organization, Cytology and Transmitters*, (Springer-Verlag, Heidelberg, Germany, 1977).
64. Chow, B.Y., Boyden, E.S. Optogenetics and translational medicine. *Sci Transl Med.* 5, 177ps5. (2013)
65. Creed, M., Pascoli, V.J., Luscher, C. Addiction therapy. Refining deep brain stimulation to emulate optogenetic treatment of synaptic pathology. *Science.* 347, 659–64 (2015).
66. Krauss, G.L. & Koubeissi, M.Z. Cerebellar and thalamic stimulation treatment for epilepsy. *Acta. Neurochir. Suppl.* 97, 347–356 (2007).
67. Krook-Magnuson, E., Szabo, G.G., C, A., M., O. & Soltesz, I. Cerebellar Directed Optogenetic Intervention Inhibits Spontaneous Hippocampal Seizures in a Mouse Model of Temporal Lobe Epilepsy. *eNeuro* 1, 1–15 (2014).
68. Engel, J., Jr. *Outcome with respect to epileptic seizures*, (Raven Press, New York, 1987).
69. Chkhenkeli, S.A., et al. Electrophysiological effects and clinical results of direct brain stimulation for intractable epilepsy. *Clin. Neuro.l Neurosurg.* 106, 318–329 (2004).
70. Sramka, M. & Chkhenkeli, I.S. Clinical experience in intraoperational determination of brain inhibitory structures and application of implanted neurostimulators in epilepsy. *Stereotact. Funct. Neurosurg.* 54–55, 56–59 (1990).
71. Sramka, M., Fritz, G., Galanda, M. & Nadvornik, P. Some observations in treatment stimulation of epilepsy. *Acta Neurochir. (Suppl.)* 23, 257–262 (1976).
72. Fisher, R.S. Therapeutic devices for epilepsy. *Ann. Neurol.* 71, 157–168 (2012).
73. Hartikainen, K.M., et al. Immediate effects of deep brain stimulation of anterior thalamic nuclei on executive functions and emotion-attention interaction in humans. *J. Clin. Exp. Neuropsychol.* 36, 540–550 (2014).

3.6. TABLES

Table 3.1 (Corresponding to Figure 3.1)

Tested data	Compared groups	*n*	*p*-value	*t*- or *F*-value	Statistical test
Differences in phase relation between CN modulation and GSWD cycle					
Phase relation	MCN IN LCN	100 67 43	0.512	*F*(2,100)=0.674	Watson-Williams multi-sample test
Differences in CN neuronal action potential firing					
Coherence	*tg* GSWD-modulated *tg* non-modulated	103 107	**<0.001**	*t*(195.9)=13.35	Independent samples t-test
Overall	wild-type *tg* GSWD-modulated interictal	94 103	**<0.001**	*F*(4,192)=68.72	MANOVA (Pillai's trace)
Firing frequency	wild-type *tg* GSWD-modulated interictal	94 103	0.095	*F*(1,195)=2.81	ANOVA (Bonferroni)
Coefficient of Variation	wild-type *tg* GSWD-modulated interictal	94 103	**<0.001**	*F*(1,195)=58.88	ANOVA (Bonferroni)
CV2	wild-type *tg* GSWD-modulated interictal	94 103	**<0.001**	*F*(1,195)=34.63	ANOVA (Bonferroni)
Burst index	wild-type *tg* GSWD-modulated interictal	94 103	**<0.001**	*F*(1,195)=2 30.86	ANOVA (Bonferroni)
Overall	wild-type *tg* non-modulated interictal	94 107	**<0.001**	*F*(4,196)=16.66	MANOVA (Pillai's trace)
Firing frequency	wild-type *tg* non-modulated interictal	94 107	0.092	*F*(1,199)=2.86	ANOVA (Bonferroni)
Coefficient of Variation	wild-type *tg* non-modulated interictal	94 107	**<0.001**	*F*(1,199)=15.13	ANOVA (Bonferroni)
CV2	wild-type *tg* non-modulated interictal	94 107	**<0.01**	*F*(1,199)=6.79	ANOVA (Bonferroni)
Burst index	wild-type *tg* non-modulated interictal	94 107	**<0.001**	*F*(1,199)=37.99	ANOVA (Bonferroni)
Overall	*tg* GSWD-modulated interictal *tg* non-modulated interictal	103 107	**<0.001**	*F*(4,205)=17.84	MANOVA (Pillai's trace)
Firing frequency	*tg* GSWD-modulated interictal *tg* non-modulated interictal	103 107	**<0.001**	*F*(1,208)=16.31	ANOVA (Bonferroni)
Coefficient of Variation	*tg* GSWD-modulated interictal *tg* non-modulated interictal	103 107	**<0.01**	*F*(1,208)=7.12	ANOVA (Bonferroni)
CV2	*tg* GSWD-modulated interictal *tg* non-modulated interictal	103 107	**<0.01**	*F*(1,208)=9.47	ANOVA (Bonferroni)
Burst index	*tg* GSWD-modulated interictal *tg* non-modulated interictal	103 107	**<0.001**	*F*(1,208)=62.6	ANOVA (Bonferroni)

Table 3.2 (Corresponding to Figure 3.2B, E–G)

Tested data	Compared groups	*n*	*p* value	*F* value	Statistical test
Effects of bilateral CN gabazine injections on CNN activity					
Overall	*tg* pre-gabazine *tg* post-gabazine	81 55	**<0.001**	$F(4,131)=39.83$	MANOVA (Pillai's trace)
Firing frequency	*tg* pre-gabazine *tg* post-gabazine	81 55	**<0.001**	$F(1,134)=37.15$	ANOVA (Bonferroni)
Coefficient of Variation	*tg* pre-gabazine *tg* post-gabazine	81 55	**<0.001**	$F(1,134)=61.21$	ANOVA (Bonferroni)
CV2	*tg* pre-gabazine *tg* post-gabazine	81 55	**<0.001**	$F(1,134)=117.63$	ANOVA (Bonferroni)
Burst index	*tg* pre-gabazine *tg* post-gabazine	81 55	**<0.01**	$F(1,134)=8.71$	ANOVA (Bonferroni)
Effects pharmacological manipulations of CN neurons on GSWDs					
GSWD occurrence	*tg* pre-saline CN *tg* post-saline CN	6	0.180		Friedman's ANOVA
	tg pre-muscimol CN *tg* post-muscimol CN	10	**<0.01**		Friedman's ANOVA
	tg pre-gabazine CN *tg* post-gabazine CN	10	**<0.01**		Friedman's ANOVA
	tg pre-muscimol cortex *tg* post-muscimol cortex	5	0.655		Friedman's ANOVA
	tg pre-gabazine cortex *tg* post-gabazine cortex	5	0.317		Friedman's ANOVA
GSWD duration	*tg* pre-saline CN *tg* post-saline CN	6	0.414		Friedman's ANOVA
	tg pre-muscimol CN *tg* post-muscimol CN	10	0.206		Friedman's ANOVA
	tg pre-gabazine CN *tg* post-gabazine CN	10	0.317		Friedman's ANOVA
	tg pre-muscimol cortex *tg* post-muscimol cortex	5	0.655		Friedman's ANOVA
	tg pre-gabazine cortex *tg* post-gabazine cortex	5	0.655		Friedman's ANOVA

Table 3.3 (Corresponding to Figure 3.2E–G)

Tested data	Compared groups	*n*	*p*-value	Statistical test
Effects pharmacological manipulations of CN neurons on GSWDs				
GSWD occurrence pre vs. post	*tg* pre-muscimol IN/LCN *tg* post-muscimol IN/LCN	6	**<0.05**	Friedman's ANOVA
	tg pre-muscimol MCN *tg* post-muscimol MCN	4	**<0.05**	Friedman's ANOVA
	tg pre-gabazine IN/LCN *tg* post-gabazine IN/LCN	5	**<0.05**	Friedman's ANOVA
	tg pre-gabazine MCN *tg* post-gabazine MCN	5	**<0.05**	Friedman's ANOVA
GSWD occurrence medial vs. lateral CN	*tg* post-muscimol IN/LCN *tg* post-muscimol MCN	6 4	0.067	Mann-Whitney *U* test
	tg post-gabazine IN/LCN *tg* post-gabazine MCN	5 5	**<0.01**	Mann-Whitney *U* test
GSWD duration pre vs. post	*tg* pre-muscimol IN/LCN *tg* post-muscimol IN/LCN	6	0.102	Friedman's ANOVA
	tg pre-muscimol MCN *tg* post-muscimol MCN	4	1.00	Friedman's ANOVA
	tg pre-gabazine IN/LCN *tg* post-gabazine IN/LCN	5	1.00	Friedman's ANOVA
	tg pre-gabazine MCN *tg* post-gabazine MCN	5	0.180	Friedman's ANOVA
GSWD duration medial vs. lateral CN	*tg* post-muscimol IN/LCN *tg* post-muscimol MCN	6 4	0.352	Mann-Whitney *U* test
	tg post-gabazine IN/LCN *tg* post-gabazine MCN	5 5	0.413	Mann-Whitney *U* test

Table 3.4

Tested data	Compared groups	*n*	*p*-value	*F*-vahie	Statistical test
Effects of bilateral CN gabazine injections on neuronal activity					
Overall	*tg* pre-gabazine IN/LCN *tg* post-gabazine IN/LCN	40 27	**<0.001**	*F*(4,62)=12.41	MANOVA (Pillai's trace)
Firing frequency	*tg* pre-gabazine IN/LCN *tg* post-gabazine IN/LCN	40 27	**<0.01**	*F*(1,65)=8.80	ANOVA (Bonferroni)
Coefficient of Variation	*tg* pre-gabazine IN/LCN *tg* post-gabazine IN/LCN	40 27	**<0.001**	*F*(1,65)=23.18	ANOVA (Bonferroni)
CV2	*tg* pre-gabazine IN/LCN *tg* post-gabazine IN/LCN	40 27	**<0.001**	*F*(1,65)=25.13	ANOVA (Bonferroni)
Burst index	*tg* pre-gabazine IN/LCN *tg* post-gabazine IN/LCN	40 27	**<0.01**	*F*(1,65)=10.22	ANOVA (Bonferroni)
Overall	*tg* pre-gabazine MCN *tg* post-gabazine MCN	41 28	**<0.001**	*F*(4,64)=40.55	MANOVA (Pillai's trace)
Firing frequency	*tg* pre-gabazine MCN *tg* post-gabazine MCN	41 28	**<0.001**	*F*(1,67)=37.53	ANOVA (Bonferroni)
Coefficient of Variation	*tg* pre-gabazine MCN *tg* post-gabazine MCN	41 28	**<0.001**	*F*(1,67)=60.04	ANOVA (Bonferroni)
CV2	*tg* pre-gabazine MCN *tg* post-gabazine MCN	41 28	**<0.001**	*F*(1,67)=153.36	ANOVA (Bonferroni)
Burst index	*tg* pre-gabazine MCN *tg* post-gabazine MCN	41 28	0.614	*F*(1,67)=0.61	ANOVA (Bonferroni)
Overall	*tg* pre-gabazine IN/LCN *tg* pre-gabazine MCN	40 41	**<0.001**	*F*(4,76)=6.28	MANOVA (Pillai's trace)
Firing frequency	*tg* pre-gabazine IN/LCN *tg* pre-gabazine MCN	40 41	0.438	*F*(4,79)=0.61	ANOVA (Bonferroni)
Coefficient of Variation	*tg* pre-gabazine IN/LCN *tg* pre-gabazine MCN	40 41	0.037	*F*(4,79)=4.51	ANOVA (Bonferroni)
CV2	*tg* pre-gabazine IN/LCN *tg* pre-gabazine MCN	40 41	0.494	*F*(4,79)=0.47	ANOVA (Bonferroni)
Burst index	*tg* pre-gabazine IN/LCN *tg* pre-gabazine MCN	40 41	**<0.001**	*F*(4,79)=13.53	ANOVA (Bonferroni)
Overall	*tg* post-gabazine IN/LCN *tg* post-gabazine MCN	27 28	**<0.001**	*F*(4,50)=4.29	MANOVA (Pillai's trace)
Firing frequency	*tg* post-gabazine IN/LCN *tg* post-gabazine MCN	27 28	0.344	*F*(4,53)=0.91	ANOVA (Bonferroni)
Coefficient of Variation	*tg* post-gabazine IN/LCN *tg* post-gabazine MCN	27 28	**≤0.001**	*F*(4,53)=13.55	ANOVA (Bonferroni)
CV2	*tg* post-gabazine IN/LCN *tg* post-gabazine MCN	27 28	**<0.01**	*F*(4,53)=10.16	ANOVA (Bonferroni)
Burst index	*tg* post-gabazine IN/LCN *tg* post-gabazine MCN	27 28	0.801	*F*(4,53)=0.64	ANOVA (Bonferroni)

Table 3.5 (Corresponding to Figure 3.3)

Tested data	Compared groups	*n*	*p*-value	*F*-value	Statistical test
Effect of optogenetic CN neuron stimulation on GSWD-related power					
Open-loop bilateral 470 nm	*tg* pre-stimulation *tg* post-stimulation	178	**<0.001**	$F(1,176)=74.87$	Repeated measures ANCOVA
Open-loop unilateral 470 nm	*tg* pre-stimulation *tg* post-stimulation	43	**<0.001**	$F(1,41)=35.25$	Repeated measures ANCOVA
590 nm	*tg* pre-stimulation *tg* post-stimulation	107	0.367	$F(1,65)=0.82$	Repeated measures ANCOVA
470 nm outside CN	*tg* pre-stimulation *tg* post-stimulation	185	0.283	$F(1,65)=1.16$	Repeated measures ANCOVA
Closed-loop bilateral 470 nm	*tg* pre-stimulation *tg* post-stimulation	227	**<0.001**	$F(1,65)=456.3$	Repeated measures ANCOVA
Closed-loop unilateral 470 nm	*tg* pre-stimulation *tg* post-stimulation	49	**<0.001**	$F(1,65)=97.58$	Repeated measures ANCOVA

Table 3.6 (Corresponding to Figure 3.4)

Tested data	Compared groups	*n*	*p*-value	*t*- or *F*-value	Statistical test
Differences in CN neuronal action potential firing					
Coherence	*C3H/HeOuJ* GSWD-modulated *C3H/HeOuJ* non-modulated	28 51	**<0.001**	$t(66.6) = 5.92$	Independent samples t-test
Firing frequency	*C3H/HeOuJ* GSWD-modulated ictal *C3H/HeOuJ* GSWD-modulated interictal	28	0.138	$F(1,27) = 2.34$	Repeated measures ANOVA (Bonferroni)
Coefficient of Variation	*C3H/HeOuJ* GSWD-modulated ictal *C3H/HeOuJ* GSWD-modulated interictal	28	0.708	$F(1,27) = 0.14$	Repeated measures ANOVA (Bonferroni)
CV2	*C3H/HeOuJ* GSWD-modulated ictal *C3H/HeOuJ* GSWD-modulated interictal	28	**<0.001**	$F(1,27) = 21.35$	Repeated measures ANOVA (Bonferroni)
Burst index	*C3H/HeOuJ* GSWD-modulated ictal *C3H/HeOuJ* GSWD-modulated interictal	28	**<0.001**	$F(1,27) = 15.64$	Repeated measures ANOVA (Bonferroni)
Effects pharmacological manipulations of CN neurons on GSWDs					
GSWD occurrence	*C3H/HeOuJ* pre-muscimol *C3H/HeOuJ* post-muscimol	4	**<0.05**		Friedman's ANOVA
GSWD duration	*C3H/HeOuJ* pre-muscimol *C3H/HeOuJ* post-muscimol	4	0.317		Friedman's ANOVA
Effect of optogenetic CN stimulation on GSWD-related power					
Open-loop bilateral 470 nm	*C3H/HeOuJ* pre-stimulation *C3H/HeOuJ* post-stimulation	37	**<0.01**	$F(1,35) = 8.17$	Repeated measures ANCOVA
Open-loop unilateral 470 nm	*C3H/HeOuJ* pre-stimulation *C3H/HeOuJ* post-stimulation	19	**<0.001**	$F(1,17) = 20.32$	Repeated measures ANCOVA

Table 3.6 (Corresponding to Figure 3.4) (*continued*)

Tested data	Compared groups	*n*	*p*-value	*t*- or *F*-value	Statistical test
590 nm in CN	*C3H/HeOuJ* pre-stimulation *C3H/HeOuJ* post-stimulation	47	0.809	$F(1,45) = 0.06$	Repeated measures ANCOVA
470 nm outside CN	*C3H/HeOuJ* pre-stimulation *C3H/HeOuJ* post-stimulation	56	0.425	$F(1,54) = 0.65$	Repeated measures ANCOVA
Closed-loop bilateral 470 nm	*C3H/HeOuJ* pre-stimulation *C3H/HeOuJ* post-stimulation	46	**<0.001**	$F(1,44) = 14.20$	Repeated measures ANCOVA
Closed-loop unilateral 470 nm	*C3H/HeOuJ* pre-stimulation *C3H/HeOuJ* post-stimulation	30	**<0.05**	$F(1,28) = 4.60$	Repeated measures ANCOVA

Table 3.7 (Corresponding to Figure 3.5)

Tested data	Compared groups	*n*	*p*-value	*F-or-value*	Statistical test
Effect of optogenetic CN stimulation on the time interval between ECoG-spikes in M1					
Stopped seizures	Median interval Stimulus related interval	153	**<0.001**	$F(1,151) = 99.80$	Repeated measures ANCOVA
Continuing seizures	Median interval Stimulus related interval	25	0.088		Friedman's ANOVA
Effect of optogenetic CN stimulation on the time interval between ECoG-spikes in S1					
Stopped seizures	Median interval Stimulus related interval	153	**<0.01**	$F(1,151) = 7.22$	Repeated measures ANCOVA
Continuing seizures	Median interval Stimulus related interval	25	0.201		Friedman's ANOVA
Predictability of stimulus related time interval by phase of stimulation onset					
Stopped seizures		153	**<0.001**	$t(152) = 3.87$	Linear regression